REPORT DOCUMENTATION PAGE

Form Approved OMB NO. 0704-0188

1. REPORT DATE (DD-MM-YYYY)	2. REPORT TYPE	3. DATES COVERED (From - To)
22-01-2015	Conference Proceeding	-

4. TITLE AND SUBTITLE

MEASURED HEAT TRANSFER IN A TRANSONIC FAN RIG AT CASING WITHIMPLICATIONS ON PERFORMANCE

5a. CONTRACT NUMBER

5b. GRANT NUMBER

ARO MI-PR--

5c. PROGRAM ELEMENT NUMBER

611102

6. AUTHORS

Mark G. Turner L, Ahmed Nemnem, Anthony Gannon, Garth Hobson, Wolfgang Sanz

5d. PROJECT NUMBER

5e. TASK NUMBER

5f. WORK UNIT NUMBER

7. PERFORMING ORGANIZATION NAMES AND ADDRESSES

Naval Postgraduate School (NPS-Monterey) 14,973.00
1 University Circle

Monterey, CA 93943 -5000

8. PERFORMING ORGANIZATION REPORT NUMBER

9. SPONSORING/MONITORING AGENCY NAME(S) AND ADDRESS (ES)

U.S. Army Research Office
P.O. Box 12211
Research Triangle Park, NC 27709-2211

10. SPONSOR/MONITOR'S ACRONYM(S)
ARO

11. SPONSOR/MONITOR'S REPORT NUMBER(S)

60039-EG.5

12. DISTRIBUTION AVAILIBILITY STATEMENT

Approved for public release; distribution is unlimited.

13. SUPPLEMENTARY NOTES

The views, opinions and/or findings contained in this report are those of the author(s) and should not contrued as an official Department of the Army position, policy or decision, unless so designated by other documentation.

14. ABSTRACT

A highly loaded transonic fan with a splittered rotor and maximum pressure ratio of 2 has been tested at the Naval Postgraduate School. Temperatures on the casing outer wall have been measured using thermocouples in order to assess the heat transfer. An axisymmetric heat transfer analysis has shown that the heat transfer downstream of the rotor through the casing leads

15. SUBJECT TERMS

Transonic Compressor, Heat Transfer, Performance

16. SECURITY CLASSIFICATION OF:			17. LIMITATION OF ABSTRACT	15. NUMBER OF PAGES	19a. NAME OF RESPONSIBLE PERSON
a. REPORT	b. ABSTRACT	c. THIS PAGE			Garth Hobson
UU	UU	UU	UU		19b. TELEPHONE NUMBER: 831-656-2888

Report Title

MEASURED HEAT TRANSFER IN A TRANSONIC FAN RIG AT CASING WITHIMPLICATIONS ON PERFORMANCE

ABSTRACT

A highly loaded transonic fan with a splittered rotor and maximum pressure ratio of 2 has been tested at the Naval Postgraduate School. Temperatures on the casing outer wall have been measured using thermocouples in order to assess the heat transfer. An axisymmetric heat transfer analysis has shown that the heat transfer downstream of the rotor through the casing leads to a overstatement of the experimental efficiency by 0.57% and 0.51% for 100% and 90% speed respectively. Just above the rotor is an abradable material that can be considered adiabatic. This heat escapes only aft of the rotor and upstream of the total pressure and total temperature probes. For rotors without an adiabatic casing, the effect would be considerably higher. In addition, heat transfer coefficients have been determined that can be used to assess other compressor applications.

Conference Name: ASME Turbo Expo 2015

Conference Date: June 15, 2015

Proceedings of ASME Turbo Expo 2015
GT2015
June 15-19, 2015, Montreal, Canada

GT2015-43482 DRAFT

MEASURED HEAT TRANSFER IN A TRANSONIC FAN RIG AT CASING WITH IMPLICATIONS ON PERFORMANCE

Mark G. Turner*
Ahmed Nemnem
Department of Aerospace Engineering
University of Cincinnati
Cincinnati, OH

Anthony Gannon
Garth Hobson
Department of Mechanical
and Aerospace Engineering,
Naval Postgraduate School
Monterey, CA

Wolfgang Sanz
Institute for Thermal Turbomachinery
and Machine Dynamics,
Graz University of Technology
Graz, Austria

ABSTRACT

A highly loaded transonic fan with a splittered rotor and maximum pressure ratio of 2 has been tested at the Naval Postgraduate School. Temperatures on the casing outer wall have been measured using thermocouples in order to assess the heat transfer. An axisymmetric heat transfer analysis has shown that the heat transfer downstream of the rotor through the casing leads to a overstatement of the experimental efficiency by 0.57% and 0.51% for 100% and 90% speed respectively. Just above the rotor is an abradable material that can be considered adiabatic. This heat escapes only aft of the rotor and upstream of the total pressure and total temperature probes. For rotors without an adiabatic casing, the effect would be considerably higher. In addition, heat transfer coefficients have been determined that can be used to assess other compressor applications.

Introduction

Compressor design, test, and 3D simulations have been based on the assumption that the endwalls are adiabatic. Only a few examples exist in the literature where this assumption was questioned and looked into. Shah and Tan[1] explored using large amounts of heat transfer to improve compressor performance and an engine cycle. Isomura et al. [2] was looking at a small centrifugal compressor where heat transfer effects become important due to the small size. Kerrobrock et al. [3] commented that heat transfer was possibly important in a compressor blow down facility, and Knapke (with others) [4, 5, 6] looked into modeling that heat transfer as part of an unsteady simulation. A study by Bruna and Turner [7] [8] looked at CFD modeling of NASA rotor 37 where a simulation did a much better job of matching the temperature profiles and efficiency when heat transfer was accounted for. Accounting for heat transfer was equal to about 1% of efficiency. The AGARD report [9] presented rotor 37 as a validation case. Every simulation assumed the walls were adiabatic, and each simulation had temperatures near the casing that were higher than those measured. Even still, the idea that heat transfer is important in a compressor is not very common. A turbine is expected to have a large amount of heat transfer and yet most 3D simulations of turbines still assume the walls are adiabatic. Denton [10] made a point in a recent paper of how important boundary conditions and geometry are in a CFD simulation, but did not even mention heat transfer.

This paper will focus on measurements made of temperatures on the outside of a transonic fan rotor casing, and how a heat transfer analysis can be used to show how much heat flux is leaving the casing. The rotor design is explained by Drayton [11] and Hobson et al. [12]. A description of the detailed testing is presented by Gannon et al. [13] which includes several tip clearance. Only data at the small tip gap has been considered in this paper.

*Address all correspondence to this author. Email: mark.turner@uc.edu

Test Configuration

A schematic of the transonic rotor at the Naval Postgraduate School is shown in Figure 1. A photo of the splittered rotor is shown in Figure 2. Five J-type thermocouples were placed at different axial positions along the casing as shown in Figure 3 to measure the casing temperatures. In addition, one thermocouple was placed in the air to measure the temperature of the air near the casing. As shown in Figure 3, the air going through the compressor is discharged into the room with the test article. The air temperature is therefore elevated and the air is rapidly moving which can promote heat transfer. Figure 4 shows the total pressure, total temperature and combination probes at the rotor exit survey plane. These probes are in direct contact with the casing and then sit in the region with high velocities from the compressor exhaust. The casing is 7075-T6 aluminum (as is the rotor and nose cone) except just above the rotor is a West Systems^{TM} 105 epoxy with a 410 Microlight^{TM} filler as shown in Figure 5. This material was used to allow for varying the tip clearance and is further explained by Gannan et al. [13]. This material just above the rotor has a very low heat transfer coefficient and is considered to be adiabatic.

Figure 2. Transonic Splittered Rotor without casing.

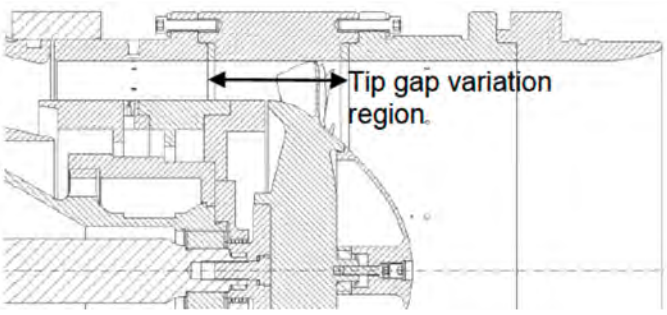

Figure 1. Transonic rotor rig cross section at the Naval Postgraduate School.

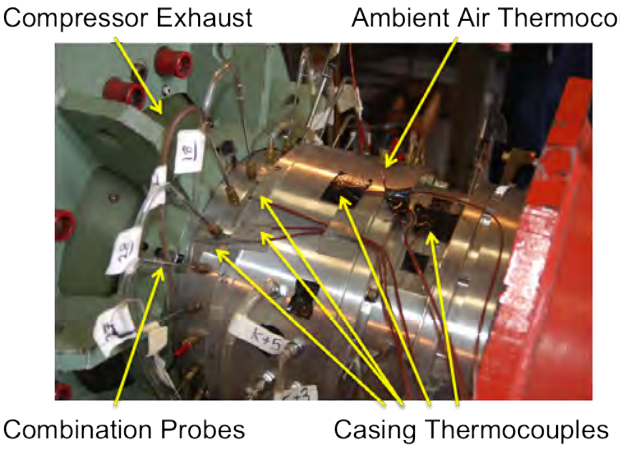

Figure 3. Outside casing of the transonic rotor showing the combination probes, thermocouples and compressor exhaust.

Figure 4. View of rotor showing combination probes.

Figure 5. Photo of inside of casing just above the rotor showing the pre-machined abradable material considered to be adiabatic.

Two test runs will be analyzed: 100% and 90% speed, both at the smallest tip gap tested (0.53 mm cold gap). Table 1 shows the running conditions for these two runs. The 90% run was taken before the 100% run while the inlet air temperature was cooler. This as well as the reduced amount of work done at 90% speed led to reduced temperatures. One of the reasons the actual mass and corrected mass are so different is that this rig throttles upstream with an inlet that drops the inlet total pressure and restricts the mass flow. This means a low back pressure is not needed and needs a lower power to run. The profiles of total temperature at the exit plane are shown in Figure 6 for both 90% and 100% speed. There is a very large peak in temperature at 88% span and then falls off near the casing. It is speculated that the gradient of temperature from the hub to about 80% span is due to the increased amount of work at higher radii, but that it increases rapidly above 80% span due to a large amount of shear work due to the high relative motion of the casing with respect to the blades and the complex tip flows interacting with shocks. Once this high temperature fluid goes downstream and the casing switches from adiabatic abradable material to high conductivity aluminum, heat is rejected from the casing and the temperatures start to decrease. This was seen in the temperature profiles presented by Bruna and Turner [7] when comparing adiabatic and isothermal solutions for rotor 37.

	100% speed	90%speed
run number	41	33
Press Ratio	1.93	1.68
efficiency	77.93%	76.94%
Actual Power (kW)	220.016	174,128
corr mass flow (kg/s)	4.543	4.096
corr speed (rpm)	26,951.7	24,290.1
actual mass flow (kg/s)	2.871	2.870
actual speed (rpm)	27,122.3	24,290.1
Inlet TT (deg C)	17.7	15.3
Exit TT_avg (deg C)	98.3	90.7
Max Exit TT (deg C)	120.2	90.7
Ambient T (deg C)	29.3	26.4

Table 1. Test Running Conditions used for heat transfer analysis. Tests run on April 17, 2014.

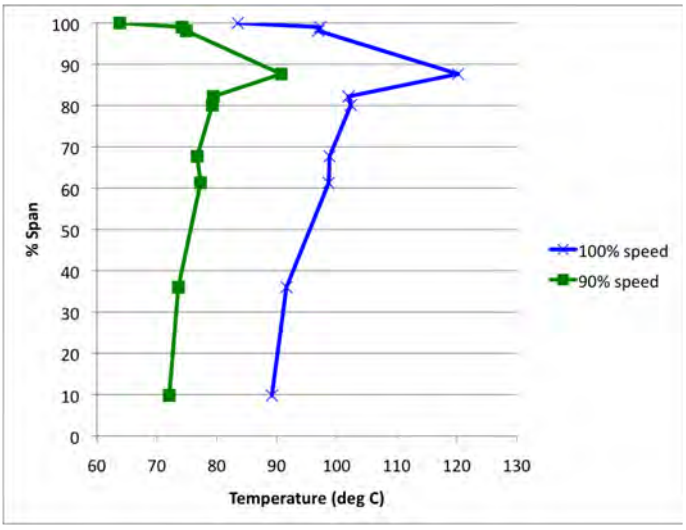

Figure 6. Exit Total Temperature Profiles for the 100% and 90% runs.

Analysis

A detailed axisymmetric heat transfer analysis was set up using Ansys Mechanical Version 14.5.7 [14]. The axisymmetric grid with cyclic boundary conditions has 201,187 nodes and 28,158 elements which is high resolution for a heat conduction problem with convection boundary conditions. The geometry of the casing is shown in Figure 7 with the boundary conditions for the 100% run shown in Figure 8. The face most upstream on this part has a loose contact with the part upstream as shown in Figure 1. That face is assumed to be adiabatic. To have an improved match to data, the probe (see the combination probe in Figure 4) heat transfer effect was modeled as an axisymmetric bump with a different convective heat transfer coefficient boundary condition. These probes are in a highly turbulent flow and allow for an increase in heat transfer out of the casing. On the outside, in three separate regions, a constant convective heat transfer coefficient has been applied using the outside temperature measured by the thermocouple. On the inside of the casing, the notch shown is where the abradable material would be so those surfaces are adiabatic. Upstream of the abradable material on the inside of the casing the measured inlet temperature is used, and a constant heat transfer coefficient again used (h= 230 W/m^2-C). Downstream of the rotor on the inside of the casing, a linear profile of convective heat transfer coefficient was used from the exit of the compressor to the interface between the abradable material and the aluminum. The average exit temperature was used. It was felt that the average would be better known for a rotor without a detailed CFD simulation. There is a very steep profile near the casing boundary so it seemed to make more sense to use a bulk average temperature. The convective heat transfer coefficients in this inner downstream region used to match the temperature data varied from 537.5 W/m^2-C to 948.7 W/m^2-C. These are very high values for h. This is due to two reasons: a constant temperature (T_exit) is used when it is postulated that the temperature is being reduce. In addition, there is high scrubbing due to the tip vortex rotating around the annulus. This effect should weaken going downstream and justifies the axial variation of h.

For 90% speed, the boundary conditions of the model are shown in Figure 9. The overall h on the downstream inner side with the linear variation was reduced by 12.5 W/m^2-C, The same variation with axial distance was used. The upstream inner region used an h=250 W/m^2-C, an increase of 20 W/m^2-C. Over most of the outside, h went from 150 to 160 W/m^2-C. At the probe, it was reduced by half from 162.5 to 80 W/m^2-C. The downstream outer region had h go from 350 to 300 W/m^2-C.

Results

The temperatures in the model on the outside of the casing as a function of the distance going upstream are shown in Figure 10. The match was achieved by setting the heat transfer coefficients to the values presented in the previous section. There are discontinuities in the plot where there are two radii at the same axial location. The match is quite good, and not many changes were needed in the values of h when going from 100% speed to 90% speed. A contour plot of the temperatures in the casing for this 100% speed case is shown in Figure 11. The match to the thermocouples as shown in Figure 10 was good so this contour plot should be representative of the temperatures throughout the casing. The material is aluminum with a high thermal conductivity. It is expected that the temperature gradients are mostly axial. The average increase in temperature for the rotor is 80.6 deg C for 100% speed. This high temperature drives the heat transfer at the outer part of the casing downstream of the rotor, and the heat goes into the room as well as a small amount back into the upstream side of the rotor. The heat flux through the casing would be normal to the constant temperature contours. The contour plot of temperature for the 90% speed case is shown in Figure 12. The min and max values have been adjusted since the overall temperature levels of this case are lower. The contours look very similar to the 100% speed case. This is not unexpected since the heat transfer physics are similar.

The heat flux downstream of the rotor where the abradable material (considered adiabatic) ends and the aluminum starts on the inside is shown in Figure 13. The red line indicates the location of the total temperature probes. Table 2 shows that the amount of heat flux at 100% speed leaving the compressor before the probe location is 1.249 kW. This is 0.57% of the overall power (actual mass flow times enthalpy rise). This makes sense given the temperature profile in Figure 6. The heat transfer has reduced the temperature right near the casing. For the 90% speed case it is 0.887 kW by the probe location or 0.51% of the overall work. By the end of the compressor, the heat flux represents nearly 1% of the power at 100% speed and 0.86% at 90% speed. For a casing that is adiabatic over the rotor, this is a lot of heat transfer that is almost always ignored.

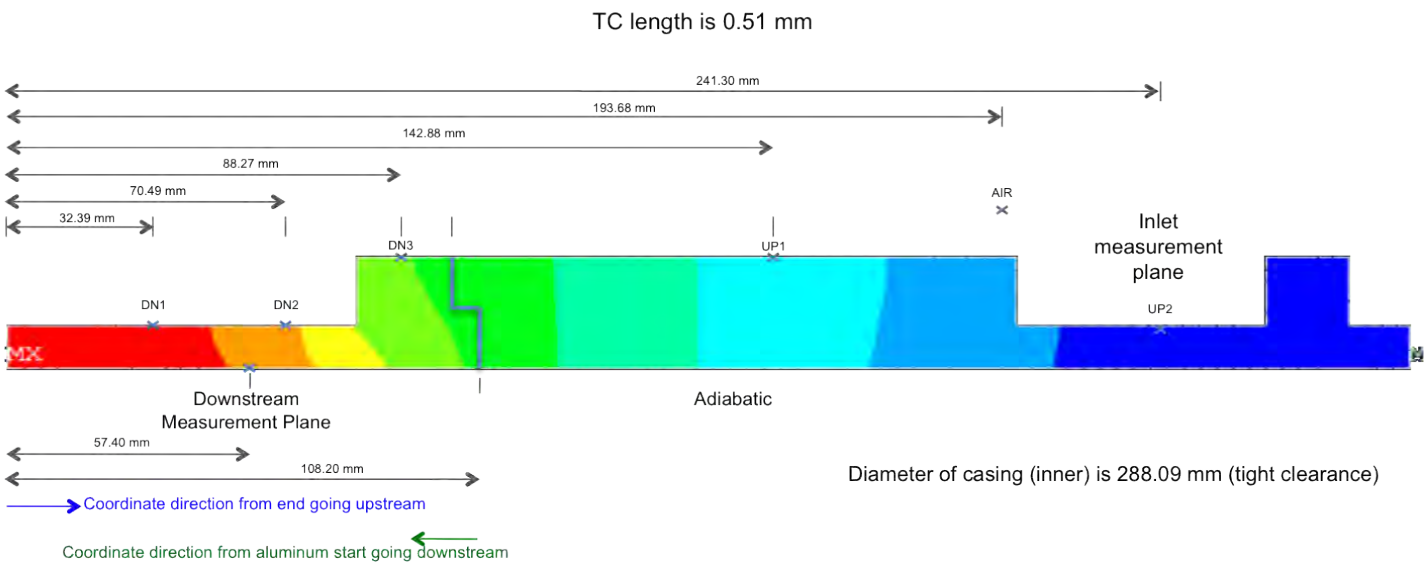

Figure 7. Key distances of model, (mm).

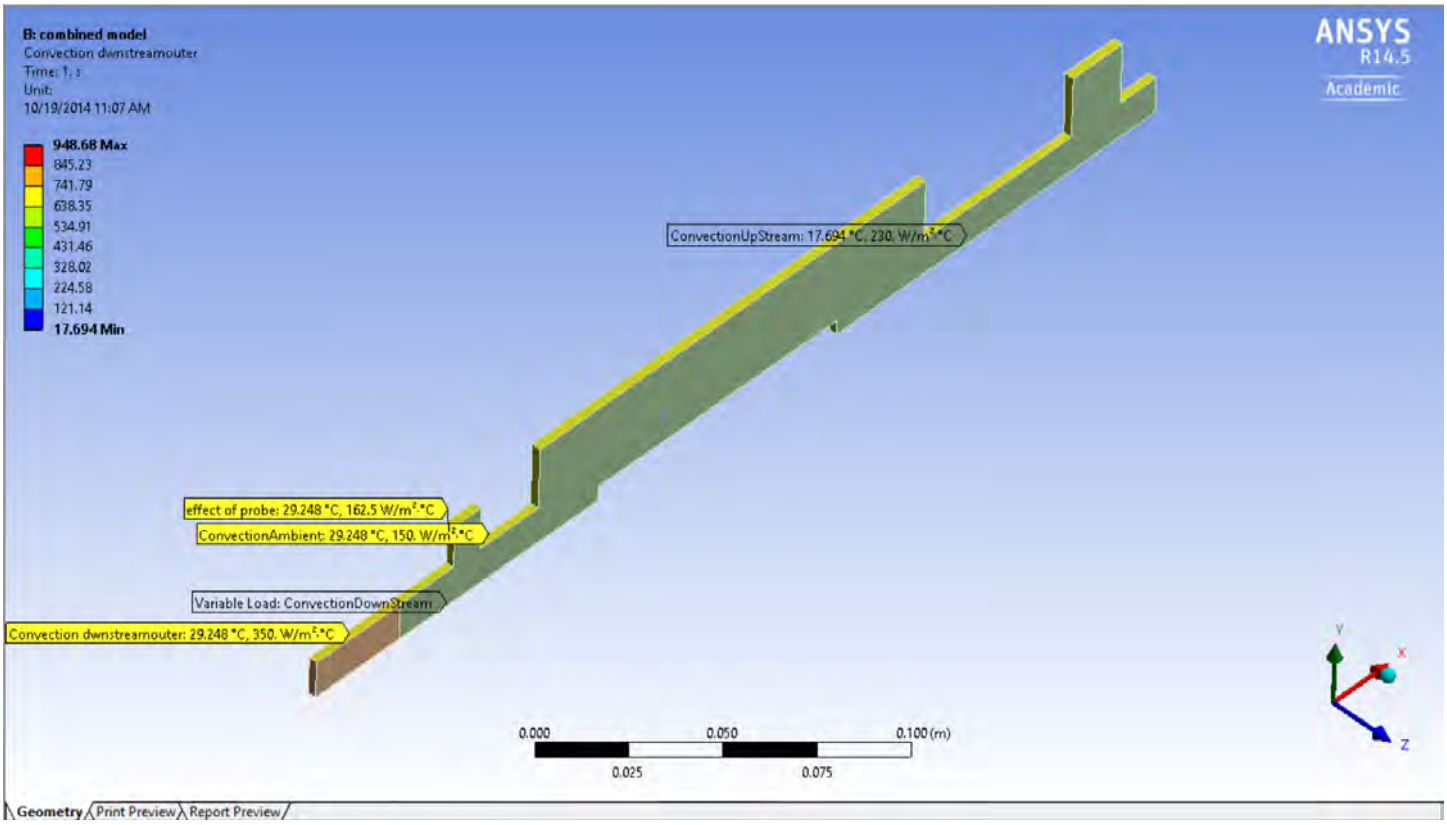

Figure 8. Boundary Conditions for the 100% speed heat transfer analysis. The heat transfer coefficient downstream of the rotor on inside casing varied linearly from 537.5 W/m^2-C to 948.7 W/m^2-C.

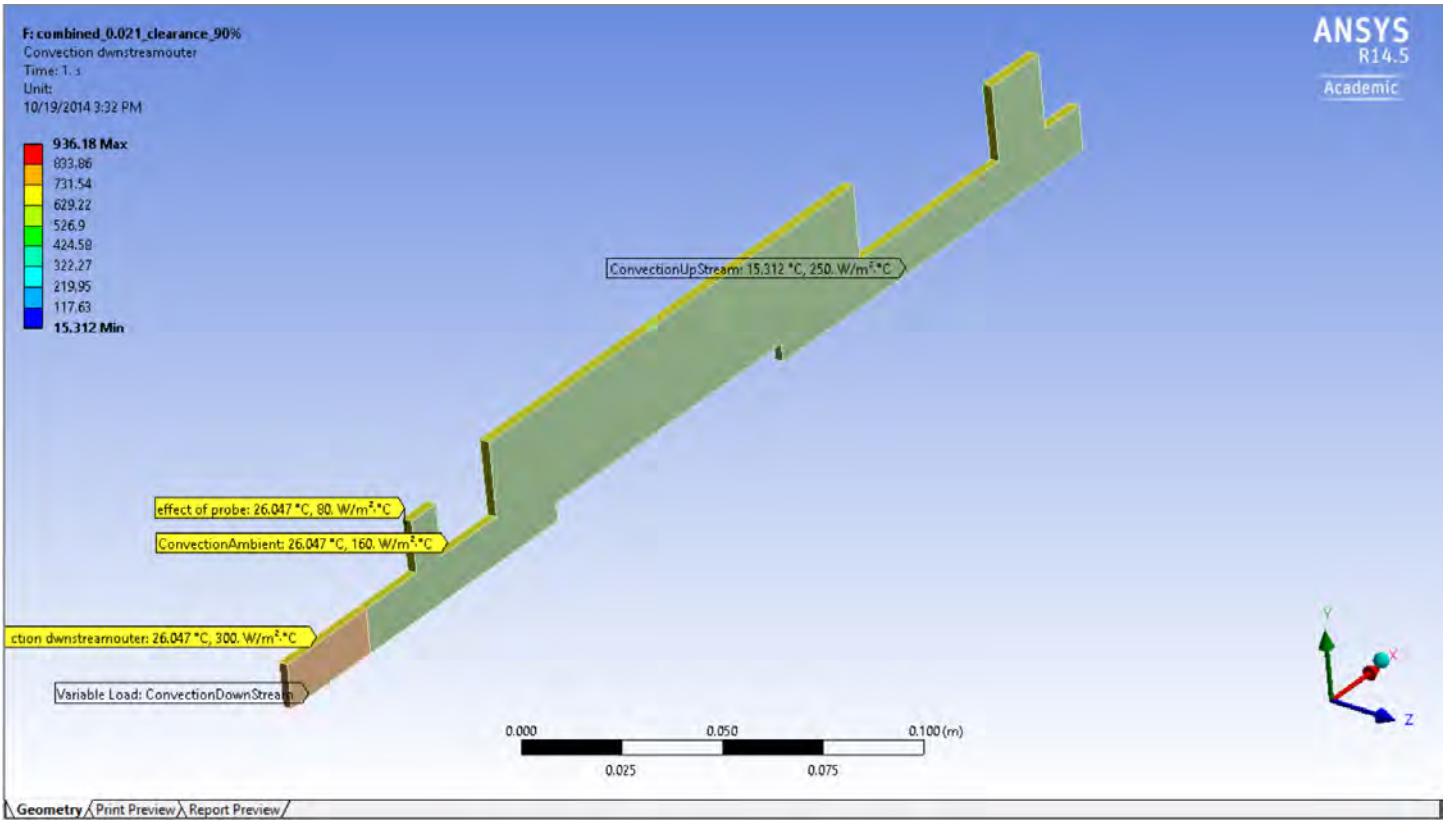

Figure 9. Boundary Conditions for the 90% speed heat transfer analysis. The heat transfer coefficient downstream of the rotor on inside casing varied linearly from 525 W/m^2-C to 936.2 W/m^2-C.

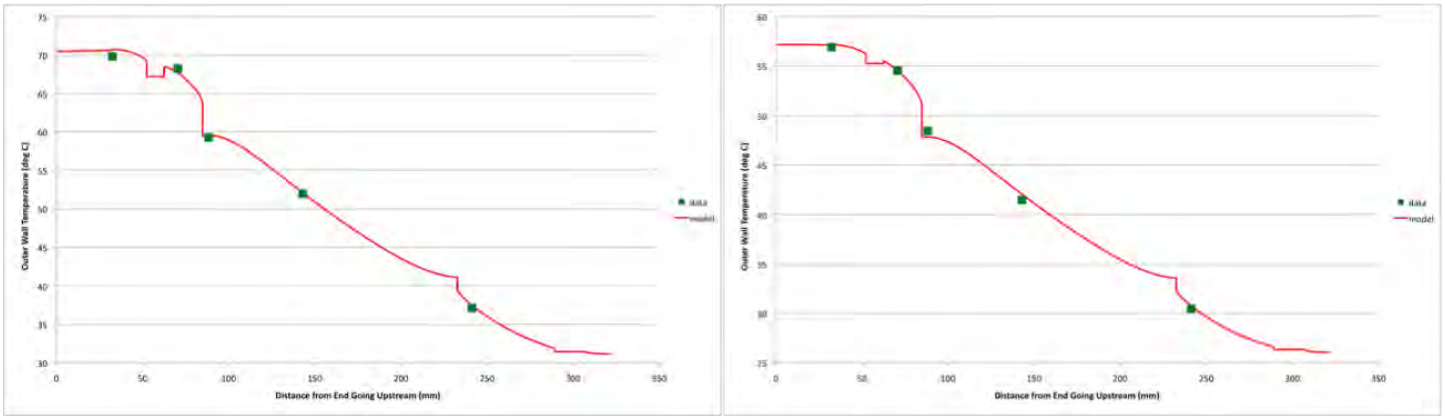

a.) 100% speed

b.) 90% speed

Figure 10. Casing outer Temperature, model compared to thermocouple measurements.

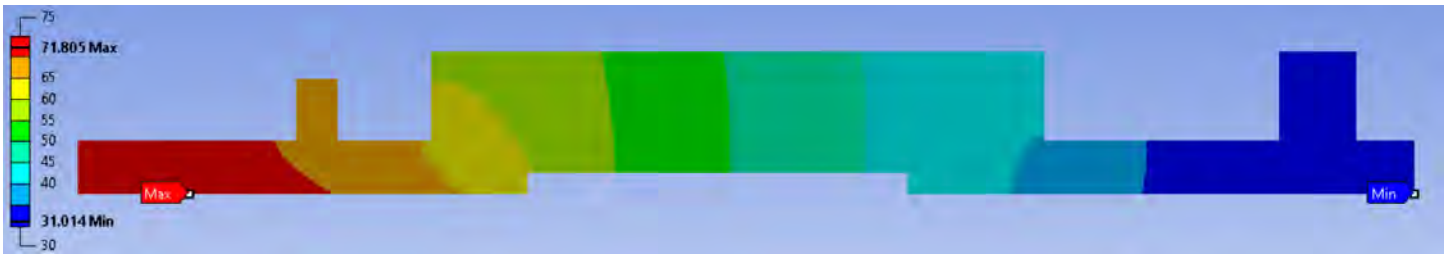

Figure 11. Contours of Temperature throughout casing for 100% speed.

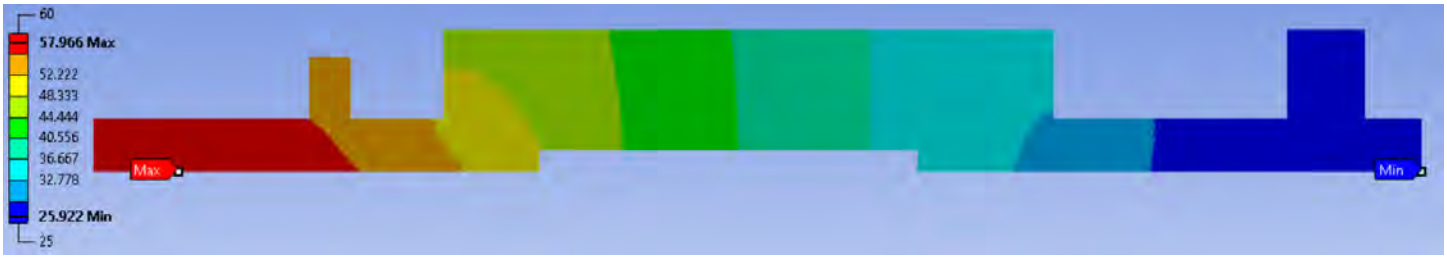

Figure 12. Contours of Temperature throughout casing for 90% speed.

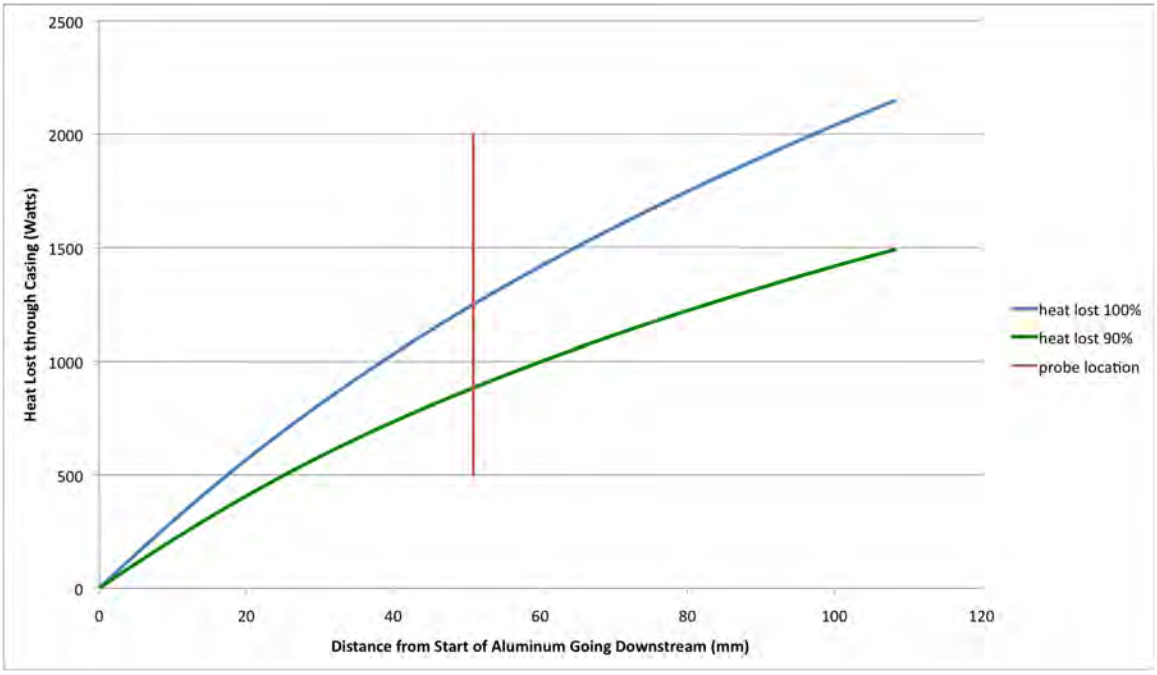

Figure 13. Heat lost through Casing for both 100% and 90% speed downstream of where abradable material stops and aluminum starts.

	100%	90%
Actual Power (kW)	220.016	174,128
Heat Lost upstream of probe (kW)	1.249	0.887
percent of heat lost upstream of probe	0.57%	0.51%
Heat Lost by compressor end (kW)	2.148	1.491
percent of heat lost by compressor end	0.98%	0.86%

Table 2. Heat lost from the inner side of the casing downstream of where the abradable material stops and aluminum starts.

Conclusions

A heat transfer analysis has been performed in a compressor casing and calibrated using measured casing metal temperatures. Based on the analysis, the implied heat flux upstream of the rotor measurement plane relative to the overall work is 0.57% at 100% speed and 0.51% at 90% speed. This means that the quoted adiabatic efficiencies are higher by these amounts. For the entire region downstream of the rotor, this heat flux to work ratio is 0.98% and 0.86% for the 100% and 90% speeds respectively. This test set up actually includes an abradable material above the rotor tip that can be considered adiabatic. For many other tests or actual hardware conditions, there would be more area for heat be transferred. The region downstream of the rotor is generally where a stator would sit, and could enhance heat transfer even more. This amount of heat transfer is not extremely large but should be accounted for when using experiments for CFD validation. It also means Conjugate Heat Transfer simulations should become more common. There is also a potential to use heat transfer to create an interstage intercooling capability for a compressor to appear more efficient for the cycle.

Acknowledgements

Thanks to John Gibson of the Turbomachinery Lab at the Naval Postgraduate School for all the support.

REFERENCES

[1] Shah, P., and Tan, C., 2005. "Effect of blade passage surface heat extraction on axial compressor performance". In ASME GT2005-68815.

[2] Isomura, K., Teramoto, S., ichi Togo, S., Hikichi, K., Endo, Y., and Tanake, S., 2006. "Effects of teynolds number and tip clearances on the performance of a centrifugal compressor at micro scale". In ASME GT2006-90637.

[3] Kerrebrock, J. L., Epstein, A. H., Merchant, A. A., Guenette, G. R., Parker, D., Onnee, J.-F., Neumayer, G., Adamczyk, J. J., and Shabbir, A., 2006. "Design and test of an aspirated counter-rotating fan". In ASME Turbo Expo 2006. ASME Paper GT-2006-90582.

[4] Knapke, R., 2011. "Unsteady analysis of a counter-rotating aspirated compressor using phase-lag and non-linear harmonic methods". Master's thesis, University of Cincinnati, Cincinnati, OH.

[5] Knapke, R., and Turner, M. G., 2013. "Detailed unsteady simulation of a counterrotating aspirated compressor with a focus on the aspiration slot and plenum". *International Journal of Rotating Machinery,* **2013**(857616), Jan, p. 17.

[6] Knapke, R., and Turner, M. G., 2013. "Unsteady simulations of a counter-rotating aspirated compressor". In ASME Paper GT2013-95209.

[7] Bruna, D., and Turner, M. G., 2013. "Isothermal boundary condition at casing applied to the rotor 37 transonic axial flow compressor". *Journal of Turbomachinery,* **135**(3), 03, pp. 034501–034501.

[8] Bruna, D., and Turner, M. G., 2013. "A rothalpy analysis for the isothermal boundary condition at casing applied to the rotor 37 transonic axial flow compressor". In ASME Paper GT2013-94595.

[9] AGARD, 1998. Cfd validation for propulsion system components. Tech. Rep. 355, AGARD, May.

[10] DENTON, J. D., 2010. "Some limitations of turbomachinery cfd". In ASME GT2010-22540.

[11] Drayton, S., 2013. "Design, test, and evaluation of a transonic axial compressor rotor with splitter blades". Phd thesis, Naval Postgraduate School, Monterey, CA 93943-5000, September.

[12] Hobson, G. V., Gannon, A. J., and Drayton, S., 2015. "Design and test of a transonic axial splittered rotor". In ASME GT2015-43005.

[13] Gannon, A. J., Hobson, G. V., Turner, M. G., and Sanz, W., 2015. "Performance of a splittered transonic rotor with several tip clearances". In ASME Paper GT2015-43799.

[14] ANSYS Inc. www.ansys.com/products/Workflow+Technology.